

Melting of the Earth's inner core

David Gubbins^{1,2}, Binod Sreenivasan³, Jon Mound¹ & Sebastian Rost¹

The Earth's magnetic field is generated by a dynamo in the liquid iron core, which convects in response to cooling of the overlying rocky mantle. The core freezes from the innermost surface outward, growing the solid inner core and releasing light elements that drive compositional convection^{1–3}. Mantle convection extracts heat from the core at a rate that has enormous lateral variations⁴. Here we use geodynamo simulations to show that these variations are transferred to the inner-core boundary and can be large enough to cause heat to flow into the inner core. If this were to occur in the Earth, it would cause localized melting. Melting releases heavy liquid that could form the variable-composition layer suggested by an anomaly in seismic velocity in the 150 kilometres immediately above the inner-core boundary^{5–7}. This provides a very simple explanation of the existence of this layer, which otherwise requires additional assumptions such as locking of the inner core to the mantle, translation from its geopotential centre^{7,8} or convection with temperature equal to the solidus but with composition varying from the outer to the inner core⁹. The predominantly narrow downwellings associated with freezing and broad upwellings associated with melting mean that the area of melting could be quite large despite the average dominance of freezing necessary to keep the dynamo going. Localized melting and freezing also provides a strong mechanism for creating seismic anomalies in the inner core itself, much stronger than the effects of variations in heat flow so far considered¹⁰.

The core responds passively to the non-uniform heat flow imposed by the mantle: it plays a purely passive role in this coupled convective system. Variations in heat flux around the core–mantle boundary (CMB), created by mantle convection, are likely to be large. They can be estimated by two independent methods, one using seismic tomography¹¹ within the supposed thermal boundary layer at the base of the mantle, and the other using mantle convection studies⁴. Both suggest variations comparable with the average heat flux. Inhomogeneous boundary conditions can produce enormous effects on core convection^{12–14}, and when background convection is small the boundary variations can aid magnetic field generation through enhanced helical motions in fluid columns¹⁵. Many geodynamo simulations have incorporated thermal boundary conditions based on seismic tomography to explain the non-axisymmetric time average of the geomagnetic field^{16–18}, low secular variation in the Pacific^{16,19}, frequency of polarity reversals²⁰, and persistent polarity transition paths during reversals²¹.

We have explored the heat flux variability on the inner-core boundary (ICB) using numerical geodynamo calculations driven by thermal convection with an inhomogeneous upper boundary heat flux and constant lower boundary temperature. The details of our dynamo model are given in the Methods. Examples using the 'tomographic' boundary condition¹¹ suffice to illustrate the possibility of inward heat flow at the lower boundary. The important parameter $q^* = (q_{\max} - q_{\min})/2q_{\text{mean}}$ measures the strength of the lateral variation in CMB heat flux relative to the average; a range from $q^* = 0.15$ to 0.45 gives dynamos that vary from one relatively unaffected by the boundary condition to one where the magnetic field is almost stationary, or statistically 'locked' to the boundary²².

Figure 1 gives the heat flux distribution on the upper and lower boundaries for a locked dynamo at $q^* = 0.45$. The pattern of heat flux on the ICB mirrors that on the CMB; negative patches of heat flux indicate heat flow into the inner core at sites of melting if this were part of the model. Figure 2 shows two snapshots and a time average for a dynamo with $q^* = 0.15$; again there are patches where the heat flux is negative despite the weaker lateral variations. Upwellings in the outer core are broad while downwellings are narrow and vertical in all these dynamos (Fig. 3), producing concentrated patches of high ICB heat flux immediately beneath high CMB heat flux. The regions of melting are therefore relatively large in comparison with the total amount of melting. We note, however, that dynamo models with different operating parameters and buoyancy profiles need not produce heat flowing into the lower boundary: a weakly convecting regime in which lateral variations at the upper boundary are allowed to propagate all the way to the lower boundary appears to be the most conducive for inner-core melting.

Three complications must be taken into account when applying the results of a thermal geodynamo simulation to the Earth. The first is the

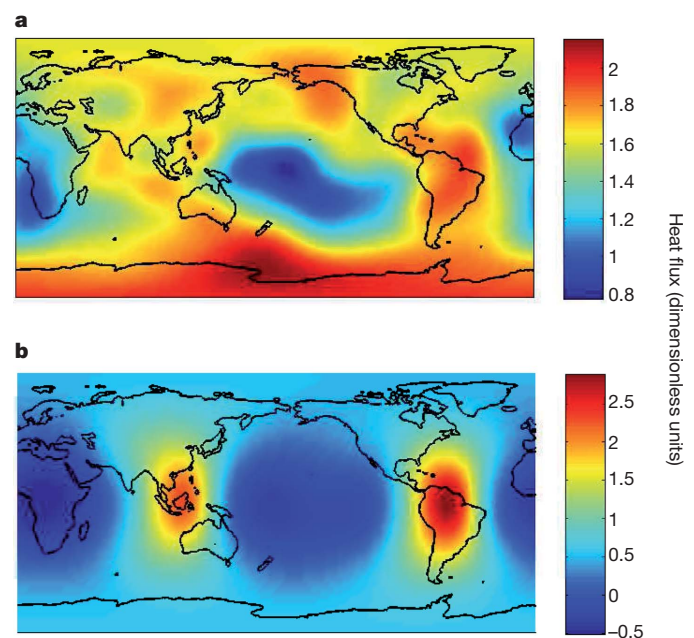


Figure 1 | Effect of mantle inhomogeneity on heat flux distribution at the inner core surface. Heat fluxes are applied to the upper boundary (a) and calculated on the constant-temperature lower boundary (b) in a geodynamo simulation where the flow is strongly coupled to the boundary thermal anomalies ($q^* = 0.45$). The range of heat flux across the upper boundary ranges from 0.77 to 2.16 dimensionless units outwards and across the lower boundary ranges from -0.51 to 2.89 dimensionless units (negative values indicate heat flux into the inner core). This model uses an Ekman number 1.2×10^{-4} , Rayleigh number 1.5 times the critical value for onset of convection, Prandtl number 1 and magnetic Prandtl number 10. (See the Methods section for definitions of these dimensionless numbers.)

¹School of Earth and Environment, University of Leeds, Leeds LS2 9JT, UK. ²IGPP, SIO, UCSD 9500 Gilman Drive, La Jolla, California 92093-0235, USA. ³Department of Mechanical Engineering, Indian Institute of Technology, Kanpur 208 016, India.

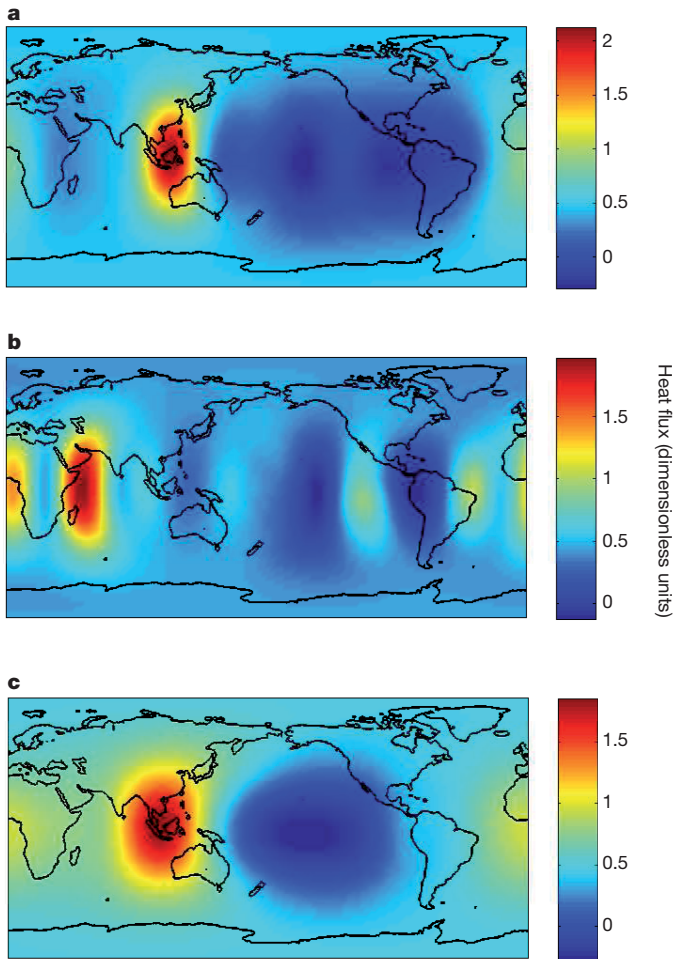


Figure 2 | Calculated heat flux on the lower boundary of a geodynamo model where $q^* = 0.15$ for the upper boundary heat flux. Panels **a** and **b** are snapshots and **c** shows the time average over several magnetic diffusion times. Heat fluxes range from -0.287 to 2.126 (**a**), -0.124 to 1.976 (**b**) and -0.276 to 1.86 (**c**) for the time average. The parameters used in this model are the same as in Fig. 1.

heat conducted down the adiabat. This was omitted from a recent mantle convection study that explored the effects of a postperovskite layer and variations in chemical composition on the heat flux across the CMB and its correlation with seismic shear wave velocity⁴. Postperovskite makes little difference to heat fluxes but lateral variations in composition, such as a subducted slab lying on the CMB, greatly increase the ratio q^* . To apply these results to core convection we must first subtract the heat conducted down the adiabatic temperature gradient. Typical estimates of the adiabatic gradient at the CMB (1 K km^{-1}) and core thermal conductivity ($k = 50 \text{ W m}^{-1} \text{ K}^{-1}$) give a conducted heat flux of 50 mW m^{-2} , comparable with q_{mean} for the mantle convection calculations. Subtracting this raises the relevant q^* dramatically because it reduces q_{mean} to nearly zero while leaving the range $q_{\text{max}} - q_{\text{min}}$ unchanged. In fact there is nothing to stop q^* becoming infinite, as it nearly does for the most realistic mantle model in the previous study⁴ (model TC-3.6, which has a compressible pyroxene content), it merely means the top of the core is thermally neutral. Most dynamo simulations have been restricted to rather low q^* because the dynamo tends to fail for large lateral heat flux variations^{15,18}. In our models with internal heating the dynamo fails by $q^* \approx 1$ but dynamos with basal heating and stratified upper layers continue to work for large q^* (ref. 23). The upper region of the Earth's fluid core is likely to be stably stratified, or at most only weakly convecting^{24,25}, and a high q^* is therefore quite possible and appropriate for the Earth. Two factors are likely to increase q^* with depth. First,

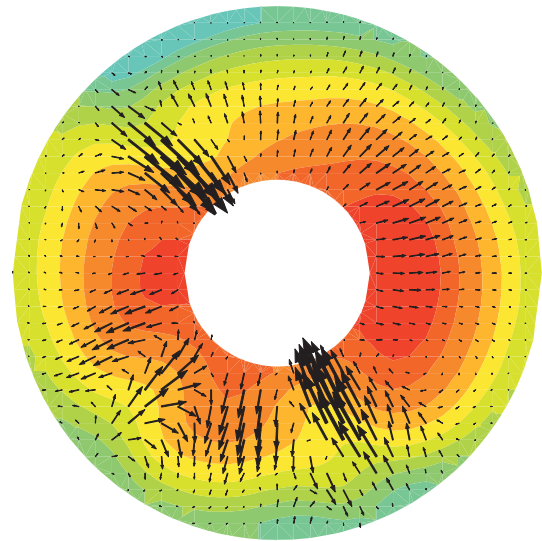


Figure 3 | Temperature (colour contours) and fluid flow (arrows) on the equatorial section for the statistically locked tomographic model ($q^* = 0.45$). The lowest temperature is blue and the highest temperature is deep red. We note the narrow downwellings beneath cold regions (the two major ones coinciding with the 'ring of fire' around the Pacific) and broad upwellings (corresponding to the mid-Pacific and African superplume). This leads to relatively large areas of negative (melting) and low-positive heat flux on the ICB and relatively small areas of strong-positive heat flux (freezing).

the adiabatic gradient weakens with depth by a factor of about three between the CMB and ICB. At the ICB the adiabatic heat flux must be added back on to the model results, reducing any heat flow into the inner core; however, the weakened adiabat makes this a relatively small effect. Second, narrow downwellings and the spherical geometry tend to concentrate the convected heat flux, increasing the lateral variations.

The second complication to consider is compositional convection. The compositional gradient is neutral or stabilizing at the CMB (assuming no passage of light elements into the mantle): convection at the top of the core is purely thermal. Compositional buoyancy tends to dominate thermal buoyancy deeper in the outer core, particularly near the ICB, as the following calculation shows. The buoyancy force is $\rho(\alpha_c c + \alpha_T T)g$, where ρ is the density, g the acceleration due to gravity, α_T the thermal expansion coefficient and α_c the compositional expansion coefficient. Compositional changes therefore have the thermal equivalent $\alpha_c c / \alpha_T$. Comparing heat and mass fluxes in the respective diffusion equations show that the conversion factor is $C_p \alpha_c / \alpha_T$, where C_p is the specific heat. Freezing 1 kg of liquid at the ICB releases L joules of latent heat and ρc kilograms of mass with thermal equivalent $C_p \alpha_c c / \alpha_T$ joules. The effective buoyancy ratio is therefore $C_p \alpha_c c / L \alpha_T = 2.3$ for a concentration $c = 0.0252$, corresponding to a density jump at the ICB of 0.6 g cm^{-3} (from PREM²⁶) assuming that 0.34 g cm^{-3} of this comes from the solid-liquid phase transition for pure iron²⁷. Compositional buoyancy dominates and will be even larger for larger ICB density jumps: 4.1 for 0.8 g cm^{-3} and 5.8 for 1.0 g cm^{-3} . Thus temperature variations are relatively unimportant in the buoyancy force near the ICB but are crucial in determining the rate of freezing, and therefore the supply of buoyancy through the release of light elements. Lateral variations in temperature imposed by the upper boundary will be carried down to the ICB by compositional convection, assisted by thermal convection, so we expect the variations on the ICB observed in the thermal or codensity geodynamo simulations to be sustained in a thermo-chemical system.

The third complication is the possible dynamic consequences of the variable-composition layer. The density gradient across the layer of freshly melted, heavy liquid is vastly steeper than anything arising from convection in the main part of the outer core: a density change of the order of 0.1 g cm^{-3} across a 150-km layer compared to a typical

convective density fluctuation of $10^{-6} \text{ g cm}^{-3}$ or less across a comparable or longer length scale, as estimated from a buoyancy–Coriolis force balance near the ICB²⁸. Such a steep density gradient would prevent downwellings from reaching the ICB, but plumes of light material produced by freezing would rise through it, drawing heavy liquid along the ICB towards the regions of freezing and maintaining mixing of the variable-composition layer. Laboratory experiments suggest that the plumes could mix the layer if the melting exceeds 20% of the freezing⁸, but the plumes on the ICB are determined by thermal, not compositional, effects. Further study is needed to understand the influence of this layer.

Regional melting of the inner core that results from heat flux variations at the CMB provides the simplest explanation of the observed variable-composition layer at the base of the outer core. It also provides a strong mechanism for seismic anomalies in the solid inner core itself because areas of melting will consist of recently exposed, precompressed material whereas areas of freezing will have layers of recently formed, unconsolidated mush. Variations in heat flux have already been invoked to explain seismic anomalies inside the inner core²⁹ but actual melting will produce even stronger effects⁷. In both cases, any correlation with mantle anomalies and persistence of locality requires the inner core and, to some extent, the core flow to be locked to the mantle. If these observations hold up to further scrutiny—in particular, if the variable-composition layer turns out not to require inner-core locking—they will provide important constraints on core evolution, convection and the dynamo.

METHODS SUMMARY

We consider a thermal convection-driven dynamo operating in an electrically conducting fluid. The Earth's outer core is modelled as a spherical shell confined between a solid iron inner core of radius r_i and an insulating mantle at radius r_o . The radius ratio r_i/r_o is taken to be that of the Earth, 0.35. In the Boussinesq approximation³⁰, the time-dependent, three-dimensional magnetohydrodynamic equations for the velocity \mathbf{u} , the magnetic field \mathbf{B} and the temperature T are solved numerically. The governing equations and numerical method are described in the Methods. The inner boundary in the model is considered to be at a fixed temperature, whereas the outer boundary is subject to a lateral variation in heat flux that has the same structure as the seismic shear-wave velocity variation in the lower mantle¹¹. This assumes shear velocity is determined by temperature and not by composition. The dominant pattern is a fast (cold) ring around the Pacific rim and slow (hot) regions beneath the Pacific and Africa (see Fig. 1).

The parameter regime used in this paper has been considered in the study of a boundary-locked dynamo^{15,22}. The Ekman number is kept sufficiently small to make the dynamics rotationally dominant, and the Rayleigh number is chosen such that free convection does not swamp the effect of the CMB lateral inhomogeneity. When the heat flux inhomogeneity ratio q^* is sufficiently large, this regime is characterized by a boundary-driven thermal wind balance¹⁵, that is, a balance between the lateral buoyancy and Coriolis forces. This force balance causes the narrow downwellings to remain locked at preferred longitudes, which can explain the quasi-stationary, non-axisymmetric flux patches in today's geomagnetic field.

Full Methods and any associated references are available in the online version of the paper at www.nature.com/nature.

Received 11 February; accepted 23 March 2011.

1. Braginsky, S. I. Structure of the F layer and reasons for convection in the Earth's core. *Dokl. Akad. Nauk. SSSR (Engl. Trans.)* **149**, 1311–1314 (1963).
2. Labrosse, S., Poirier, J.-P. & Le Mouél, J.-L. On cooling of the Earth's core. *Phys. Earth Planet. Inter.* **99**, 1–17 (1997).
3. Nimmo, F., Price, G. D., Brodholt, J. & Gubbins, D. The influence of potassium on core and geodynamo evolution. *Geophys. J. Int.* **156**, 363–376 (2004).

4. Nakagawa, T. & Tackley, P. J. Lateral variations in CMB heat flux and deep mantle seismic velocity caused by a thermal-chemical-phase boundary layer in 3D spherical convection. *Earth Planet. Sci. Lett.* **271**, 348–358 (2008).
5. Souriau, A. & Poupinet, G. The velocity profile at the base of the liquid core from PKP(BC+Cdiff) data: an argument in favor of radial inhomogeneity. *Geophys. Res. Lett.* **18**, 2023–2026 (1991).
6. Song, X. D. & Helmlinger, D. V. Velocity structure near the inner core boundary from waveform modeling. *J. Geophys. Res.* **97**, 6573–6586 (1992).
7. Monnereau, M., Calvet, M., Margerin, L. & Souriau, A. Lopsided growth of Earth's inner core. *Science* **328**, 1014–1017 (2010).
8. Alboussière, T., Deguen, R. & Melzani, M. Melting-induced stratification above the Earth's inner core due to convective translation. *Nature* **466**, 744–747 (2010).
9. Gubbins, D., Masters, G. & Nimmo, F. A thermochemical boundary layer at the base of Earth's outer core and independent estimate of core heat flux. *Geophys. J. Int.* **174**, 1007–1018 (2008).
10. Aubert, J., Amit, H. & Hulot, G. Detecting thermal boundary control in surface flows from numerical dynamos. *Phys. Earth Planet. Inter.* **160**, 143–156 (2007).
11. Masters, T. G., Johnson, S., Laske, G. & Bolton, H. F. A shear-velocity model of the mantle. *Phil. Trans. R. Soc. Lond. A* **354**, 1385–1411 (1996).
12. Zhang, K. & Gubbins, D. Convection in a rotating spherical fluid shell with an inhomogeneous temperature boundary condition at finite Prandtl number. *Phys. Fluids* **8**, 1141–1148 (1996).
13. Zhang, K. & Gubbins, D. Scale disparities and magnetohydrodynamics in the Earth's core. *Phil. Trans. R. Soc. Lond. A* **358**, 899–920 (2000).
14. Gibbons, S. & Gubbins, D. Convection in the Earth's core driven by lateral variations in the core-mantle boundary heat flux. *Geophys. J. Int.* **142**, 631–642 (2000).
15. Sreenivasan, B. On dynamo action produced by boundary thermal coupling. *Phys. Earth Planet. Inter.* **177**, 130–138 (2009).
16. Bloxham, J. The effect of thermal core-mantle interactions on the paleomagnetic secular variation. *Phil. Trans. R. Soc. Lond. A* **358**, 1171–1179 (2000).
17. Christensen, U., Olson, P. & Glatzmaier, G. A. A dynamo model interpretation of geomagnetic field structures. *Geophys. Res. Lett.* **25**, 1565–1568 (1998).
18. Olson, P. & Christensen, U. R. The time-averaged magnetic field in numerical dynamos with non-uniform boundary heat flow. *Geophys. J. Int.* **151**, 809–823 (2002).
19. Christensen, U. R. & Olson, P. Secular variation in numerical geodynamo models with lateral variations of boundary heat flow. *Phys. Earth Planet. Inter.* **138**, 39–54 (2003).
20. Glatzmaier, G. A., Coe, R. S., Hongre, L. & Roberts, P. H. The role of the Earth's mantle in controlling the frequency of geomagnetic reversals. *Nature* **401**, 885–890 (1999).
21. Kutzner, C. & Christensen, U. R. Simulated geomagnetic reversals and preferred virtual geomagnetic pole paths. *Geophys. J. Int.* **157**, 1105–1118 (2004).
22. Gubbins, D., Willis, A. P. & Sreenivasan, B. Correlation of Earth's magnetic field with lower mantle thermal and seismic structure. *Phys. Earth Planet. Inter.* **162**, 256–260 (2007).
23. Sreenivasan, B. & Gubbins, D. Dynamos with weakly convecting outer layers: implications for core–mantle boundary interaction. *Geophys. Astrophys. Fluid Dyn.* **102**, 395–407 (2008).
24. Buffett, B. A. & Seagle, C. T. Stratification of the top of the core due to chemical interactions with the mantle. *J. Geophys. Res.* **115**, B04407 (2010).
25. Helffrich, G. & Kaneshima, S. Outer-core compositional stratification from observed core wave speed profiles. *Nature* **468**, 807–810 (2010).
26. Dziewonski, A. M. & Anderson, D. L. Preliminary Reference Earth Model. *Phys. Earth Planet. Inter.* **25**, 297–356 (1981).
27. Gubbins, D., Alfè, D., Masters, T. G. & Price, D. Gross thermodynamics of 2-component core convection. *Geophys. J. Int.* **157**, 1407–1414 (2004).
28. Moffatt, H. K. & Loper, D. E. The magnetostrophic rise of a buoyant parcel in the Earth's core. *Geophys. J. Int.* **117**, 394–402 (1994).
29. Aubert, J., Amit, H., Hulot, G. & Olson, P. Thermochemical flows couple the Earth's inner core growth to mantle heterogeneity. *Nature* **454**, 758–761 (2008).
30. Sreenivasan, B. A buoyant flow structure in a magnetic field: quasi-steady states and linear–nonlinear transitions. *Phys. Lett. A* **372**, 5471–5478 (2008).

Author Contributions B.S. set up the geodynamo model and performed the calculations that form the basis of this paper. All four authors discussed the results and contributed to the text of the manuscript.

Author Information Reprints and permissions information is available at www.nature.com/reprints. The authors declare no competing financial interests. Readers are welcome to comment on the online version of this article at www.nature.com/nature. Correspondence and requests for materials should be addressed to B.S. (bsreeni@iitk.ac.in).

METHODS

Numerical dynamo model. We consider a thermal convection-driven dynamo in which an electrically conducting fluid is confined between two concentric, co-rotating spherical surfaces. The radius ratio r_i/r_o is chosen to be that of the Earth, 0.35. In the Boussinesq approximation³⁰, the time-dependent, three-dimensional magnetohydrodynamic equations for the velocity \mathbf{u} , the magnetic field \mathbf{B} and the temperature T are solved numerically³¹. The governing dimensionless equations are:

$$\frac{E}{\text{Pm}} \left(\frac{\partial \mathbf{u}}{\partial t} + (\nabla \times \mathbf{u}) \times \mathbf{u} \right) + 2\hat{\mathbf{z}} \times \mathbf{u} = -\nabla p + \text{Ra Pm Pr}^{-1} T \mathbf{r} + (\nabla \times \mathbf{B}) \times \mathbf{B} + E \nabla^2 \mathbf{u} \quad (1)$$

$$\frac{\partial \mathbf{B}}{\partial t} = \nabla \times (\mathbf{u} \times \mathbf{B}) + \nabla^2 \mathbf{B} \quad (2)$$

$$\frac{\partial T}{\partial t} + (\mathbf{u} \cdot \nabla) T = \text{Pm Pr}^{-1} \nabla^2 T \quad (3)$$

$$\nabla \cdot \mathbf{u} = \nabla \cdot \mathbf{B} = 0 \quad (4)$$

The dimensionless groups in the above equations are the Ekman number, $E = \nu/2\Omega D^2$, the Prandtl number, $\text{Pr} = \nu/\kappa$, the magnetic Prandtl number, $\text{Pm} = \nu/\eta$ and the ‘modified’ Rayleigh number $\text{Ra} = g\alpha\beta_i D^3/2\Omega\kappa$, which is the product of the conventional Rayleigh number and the Ekman number. The definition of the Rayleigh number depends on the basic state (conductive) profile in the model (see below). In the above dimensionless groups, ν is the kinematic viscosity, κ is the thermal diffusivity, η is the magnetic diffusivity, D is the gap-width of the spherical shell, Ω is the angular velocity of rotation, g is the gravitational acceleration, α is the coefficient of thermal expansion and β_i is a constant that determines the basic state temperature profile, T_0 . The Ekman number is a

measure of the rotation rate and the Rayleigh number represents the strength of convective buoyancy in the problem. Our models use an Ekman number of $E = 1.2 \times 10^{-4}$, a Rayleigh number of 1.5Ra_c , where Ra_c is the critical Rayleigh number for onset of nonmagnetic convection, a Prandtl number $\text{Pr} = 1$ and magnetic Prandtl number $\text{Pm} = 10$.

No-slip boundary conditions are imposed on the flow at the ICB and at the CMB. The inner core is considered to be at a fixed temperature and electrically conducting. The isothermal condition at the ICB is reasonable for a solid core of high thermal conductivity. However, compositional buoyancy in the form of light-element release over areas of freezing can complicate the boundary condition at the ICB. The upper boundary in the model is maintained electrically insulating to mimic the mantle and subject to a lateral variation in heat flux that has the same structure as the seismic shear-wave velocity variation in the lower mantle. The basic state temperature profile imposed in the model represents a uniform distribution of heat sources, and is given by $T_0(r) = \beta_i(r_i^2 - r^2)/2$, where r_i is the inner radius and β_i is related to a prescribed, uniform heat source Q_s as follows: $\beta_i = Q_s/3\kappa$.

The velocity and magnetic field vectors are expressed in terms of poloidal and toroidal scalars, as follows:

$$\begin{aligned} \mathbf{u} &= \nabla \times \nabla \times [P_u \mathbf{r}] + \nabla \times [T_u \mathbf{r}] \\ \mathbf{B} &= \nabla \times \nabla \times [P_B \mathbf{r}] + \nabla \times [T_B \mathbf{r}] \end{aligned} \quad (5)$$

whereby the continuity equations (4) are satisfied. The standard numerical method used here involves expanding the above four scalar variables and the temperature T in spherical harmonics in latitude θ and longitude ϕ , and time-stepping the spectral coefficients. Finite differences are used in the radial direction. The numerical integration of the equations is performed for at least five magnetic diffusion times.

31. Sreenivasan, B. & Jones, C. A. The role of inertia in the evolution of spherical dynamos. *Geophys. J. Int.* **164**, 467–476 (2006).